Field-dependent nonelectronic contributions to thermal conductivity in a metallic ferromagnet with low Gilbert damping

M. R. Natale, D. J. Wesenberg, Eric R. J. Edwards, Hans T. Nembach, Justin M. Shaw, and B. L. Zink

Phys. Rev. Materials **5**, L111401 — Published 23 November 2021

DOI: 10.1103/PhysRevMaterials.5.L111401

Field-Dependent Non-Electronic Contributions to Thermal Conductivity in a Metallic Ferromagnet with Low Gilbert Damping

M. R. Natale,[1] D. J. Wesenberg,[1] Eric R. J. Edwards,[2]
Hans T. Nembach,[2,3] Justin M. Shaw,[2] and B. L. Zink[1,*]

[1]*Department of Physics and Astronomy,*
University of Denver, Denver, CO 80208 USA

[2]*Quantum Electromagnetics Division,*
National Institute of Standards and Technology, Boulder, CO 80305 USA

[3]*JILA, University of Colorado, Boulder, CO 80309 USA*

(Dated: November 15, 2021)

Abstract

Heat conduction in metals is typically dominated by electron transport, since electrons carry both charge and heat. In magnetic metals magnons, or spin waves, excitations of the magnetic order, can be used to transport information. Heat conduction via magnons has been previously shown mostly for insulating magnets with low Gilbert damping and resulting long spin wave lifetimes, where conduction electrons cannot contribute. Here we show that thin films of properly optimized metallic ferromagnetic alloys show significant non-electronic contributions to heat conduction, which furthermore depend on the direction of an applied magnetic field. These measurements are enabled by micromachined thermal isolation platforms optimized for thermal conductivity measurements of thin film systems. Electrical conductivity measurements on exactly the same samples allows application of the Wiedemann-Franz relation, which shows large non-electronic contributions to thermal conductivity for the cobalt-iron alloy with 25% Co. This composition has been shown to have exceptionally low damping for a metallic ferromagnet. The thermal conductivity of a 75 nm thick film of the 25% Co alloy changes by more than 20% at some temperatures, while a reference sample with 50% cobalt that has much higher damping shows no field direction dependence. Our measurements indicate that applied magnetic fields alter the magnon lifetimes in these films and that these magnons contribute to thermal conductivity in this metallic magnetic alloy with low Gilbert damping.

The transport properties of metals are typically dominated by electrons, which carry energy as well as charge, leading to the well-known Wiedemann-Franz (WF) relation between electrical and thermal conductivity, $k_{\mathrm{el}}/\sigma = LT$[1–3]. Here k_{el} is the thermal conductivity due to electrons, σ is the electrical conductivity, T is the absolute temperature, and L is the Lorenz number, which is determined only by fundamental constants in simple theories of metals. Phonons also carry heat, and though recent theories suggest this contribution could be larger than traditionally thought for metals [4–7], phonon contributions are most commonly observed only when σ is strongly reduced, typically in thin films or nanostructures [8–11]. In a magnetically ordered system, energy can also be carried by magnons, the quantized spin waves that are the fundamental perturbations of the magnetic forces between neighboring spins. Magnon contributions to spin transport have been proven in insulators

* barry.zink@du.edu

[12–18] and metals [19–22]. Heat transport via magnons has been reported for insulators [23–29], with only a few studies of bulk materials at very low temperature in high magnetic field discussing magnon contributions to heat flow in metals [30–33]. Measurements of the magnon contribution to thermal conductivity, k, are more common in insulators, and so far much more difficult in metals, due to relatively strong electron-magnon scattering that typically leads to short magnon lifetimes in a metallic FM. However, recent computational work suggests that magnon thermal conductivity contributes more to a metallic ferromagnet (FM) than previously known [34, 35], and both theory [36–39] and experiment [40, 41] have renewed interest in the role of magnons in the transport and thermoelectric properties of metals. However, contributions of magnons to k in thin film metallic ferromagnets and at any $T > 5$ K have still never been demonstrated to our knowledge.

The earliest demonstration of magnon k focused on the THz magnons in magnetic insulator yttrium iron garnet (YIG), a system where α is exceptionally low, often reaching ~ 0.0001 in bulk crystals. This leads to long-lived spin wave dynamics [43], which allows heat [29] and spin [12–15, 17, 18] to be transported by magnons. α is typically on the order of 0.01 for metallic ferromagnets where conduction electron-magnon interactions are frequent. However, recent work has shown that with optimal tuning of alloy composition and growth conditions, metallic or half-metallic thin films can reach α comparable to or below that seen in magnetic insulators [42, 44–48]. These materials, including the cobalt-iron alloys, Co_xFe_{1-x}, are of great interest for spin wave transport [49], and have been recently investigated for magnon drag thermopower contributions in bulk form [50], and using suspended Si-N membrane thermal isolation platforms for thermopower and k [51]. Both papers show significant magnon drag thermopower contributions, and Srichandan *et al.* show large non-electronic contributions to k, as we will show, by examination of L. However, Srichandan *et al.* explained these based on theoretical predictions of electronic effects, and did not interpret their high k as evidence of magnons carrying heat in a metal.

In this letter, we present results from heat and charge transport measurements of optimized Co_xFe_{1-x} polycrystalline thin films that show evidence of magnon contributions to k in this low-damping metallic ferromagnet. The strongest evidence for magnon k comes from a magnetic-field direction dependence that is large in the alloy with lowest damping, and vanishing in an alloy with more typical damping. Comparison with the anisotropic magnetoresistance (AMR) measured on the same samples shows that these field effects in the

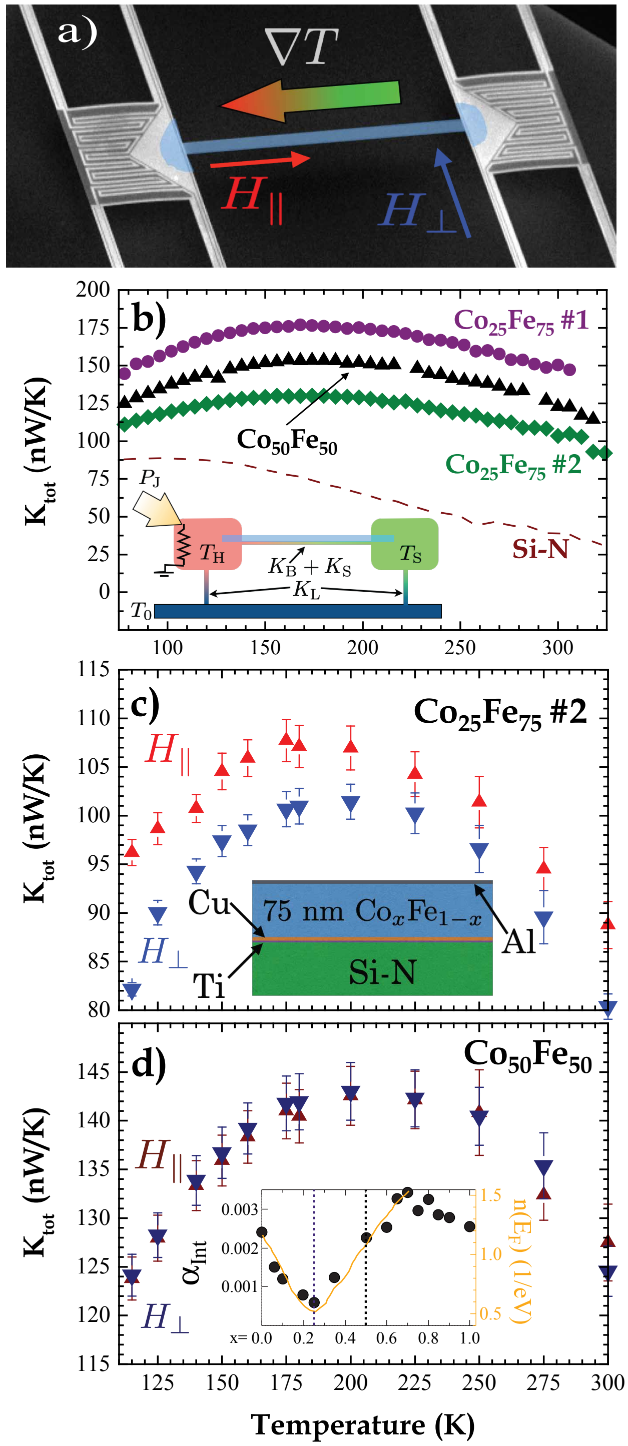

FIG. 1. **a)** Oblique angle scanning electron micrograph of the Si-N platform, with ∇ T, $H_{\|}$ and $H_{\perp}$ and sample area (blue shading) shown. The length and width of the sample are 2040 μm and 88 μm, respectively. **b)** K_{tot} vs. T for the Si-N background and three $\mathrm{Co}_x\mathrm{Fe}_{1-x}$ films. *Inset:* Thermal model used to determine K_{tot}. **c)** K_{tot} vs. T for $H_{\|}$ and $H_{\perp}$ for the low-α sample $\mathrm{Co}_{25}\mathrm{Fe}_{75}$ #2. *Inset:* Schematic side view of the sample layers. **d)** K_{tot} vs. T for $H_{\|}$ and $H_{\perp}$ for the reference sample $\mathrm{Co}_{50}\mathrm{Fe}_{50}$ shows no dependence on field direction. *Inset:* α (left axis) and density of states (right axis) vs. x [42]. Dashed lines indicate the two x studied here.

low-damping alloy are much larger than any modification based on purely electronic effects, reaching levels comparable to the best known thermal switching systems [52].

Achieving and optimizing low α in a metallic FM requires tuning of the crystal structure by thin-film growth techniques [42, 46, 47, 53]. The films studied here were prepared via DC magnetron sputtering at an Ar pressure of approximately 0.6 Pa (5×10^{-3} Torr) and chamber base pressure of 5×10^{-6} Pa (4×10^{-8} Torr). The alloy is co-sputtered from dual elemental targets (Co and Fe) with deposition rates calibrated by X-ray reflectometry. The total deposition rate is kept to 0.25 nm/s. Samples are grown with a Ti(3 nm)/Cu(5nm) seed layer to promote a BCC structure and an Al(5nm) capping layer to limit oxidation. This structure also minimizes extrinsic damping mechanisms for in-plane fields [54]. The thermal isolation platforms and other Si-N coated Si substrates for supporting characterization are held near room temperature during the sputtering.

Since thin film deposition is required to achieve low α, probing k due to magnons requires thermal measurements on thin films. These measurements are normally difficult due to the enormous background from the supporting substrate. Here we use a micromachined thermal isolation platform where a 500 nm thick amorphous silicon-nitride membrane sample platform is supported between two islands with lithographically patterned heaters, thermometers, and leads[9, 55–57]. Fig. 1a) is a scanning electron micrograph of an example platform, where the direction of the applied in-plane thermal gradient, ∇T, and the relative direction of applied magnetic fields, $H_{\parallel}$ and $H_{\perp}$ are shown. The removal of all bulk heat sinks allows use of the simple thermal model shown inset in Fig. 1b), where the two islands at temperatures T_H and T_S are bridged by the thermal conductance of the Si-N sample platform, $K_{\rm B}$, and this structure is in turn connected to the thermal bath by conductances of the supporting legs and leads, $K_{\rm L}$. Application of a series of currents to the island heater and measurement of T for each island in steady state allows calculation of K_B using this model as described in the Supplemental Materials[58], and elsewhere [9, 55–57].

When a sample is added, the thermal conductance between the islands becomes $K_{\rm tot} = K_{\rm B} + K_{\rm s}$, and we determine the sample thermal conductivity $k_{\rm film}$ from K_s such that $k_{\rm film} = K_{\rm s} l/(wt)$, where l, w, and t are the film length, width, and thickness, respectively. Fig. 1b) shows $K_{\rm tot}$ as a function of the average sample platform temperature, T, for a blank sample platform (Si-N), and three Co_xFe_{1-x} alloy films. All three films add large contributions to the Si-N background. As shown inset in Fig. 1d), both α and the density of electronic states at the Fermi level, $n(E_{\mathrm{F}})$ vary with x, and both are minimum near $x = 0.25$. Two films, labeled $Co_{25}Fe_{75}$ #1 and #2, were prepared with intended alloy composition near the minimum for both α and the electronic density of states at the Fermi level, while the third, labeled $Co_{50}Fe_{50}$ has an alloy composition that, while maintaining similar saturation magnetization and spin-orbit coupling, results in more typical α for a metallic FM and also has a larger $n(E_{\mathrm{F}})$. This sample thus serves as an important reference as we investigate k related to long-lived spin dynamics, as only α and DOS near E_{F} change meaningfully between the two alloys.

In Fig. 1c) and d) we compare K_{tot} measured in a saturating 400 Oe in-plane magnetic field applied in two different directions for a low-damping alloy sample and typical-damping alloy sample as a function of T. Here $Co_{25}Fe_{75}$ #2 shows a large difference in K_{tot} when the magnetization, $\vec{M}$, is aligned parallel to ∇T compared to when $\vec{M} \perp \nabla T$. In stark contrast, $Co_{50}Fe_{50}$ has exactly the same K_{tot} regardless of field orientation within estimated experimental uncertainty. This dramatically demonstrates the importance of spin dynamics for heat flow in these samples, as the change in orientation of $\vec{M}$ in this thin film geometry changes the magnon dispersion relations but should not strongly affect either the phonon or electron degrees-of-freedom. As discussed below, the relative alignment of $\vec{M}$ and applied current direction changes electron spin-orbit scattering which causes the AMR. However, these changes are a fraction of a percent at best; far smaller than the $10-20\%$ change in K_{tot} apparent in Fig. 1c).

Fig. 2a) plots the measured L vs. T for the three Co_xFe_{1-x} samples. Because we measure k and σ on exactly the same sample, the film geometry cancels in L, such that the values shown are determined from $L = K_{\mathrm{S}}R/T$, removing a large source of uncertainty. The dashed line labeled L_{o} indicates the free-electron Sommerfeld value, $L_o = 2.45 \times 10^{-8}$ WΩ/K^2. Slight deviations from this value both for thin films [9] and bulk metals[3] are fairly common. In agreement with the one prior report for thin films [51], we see large positive deviations from L_o indicating additional contributions to k for both $Co_{25}Fe_{75}$ films. In contrast, the higher-damping $Co_{50}Fe_{50}$ film agrees well with L_o showing only slight reduction at some T. This is very similar to results for non-magnetic thin films measured with the same techniques [9]. We plot k vs. T for each film, compared with the predicted k_{el} made using the WF law with L_o in Fig. 2b). Here we see that k is relatively low for a metal, and comparable in overall magnitude to values we previously measured for Permalloy [9], though Permalloy

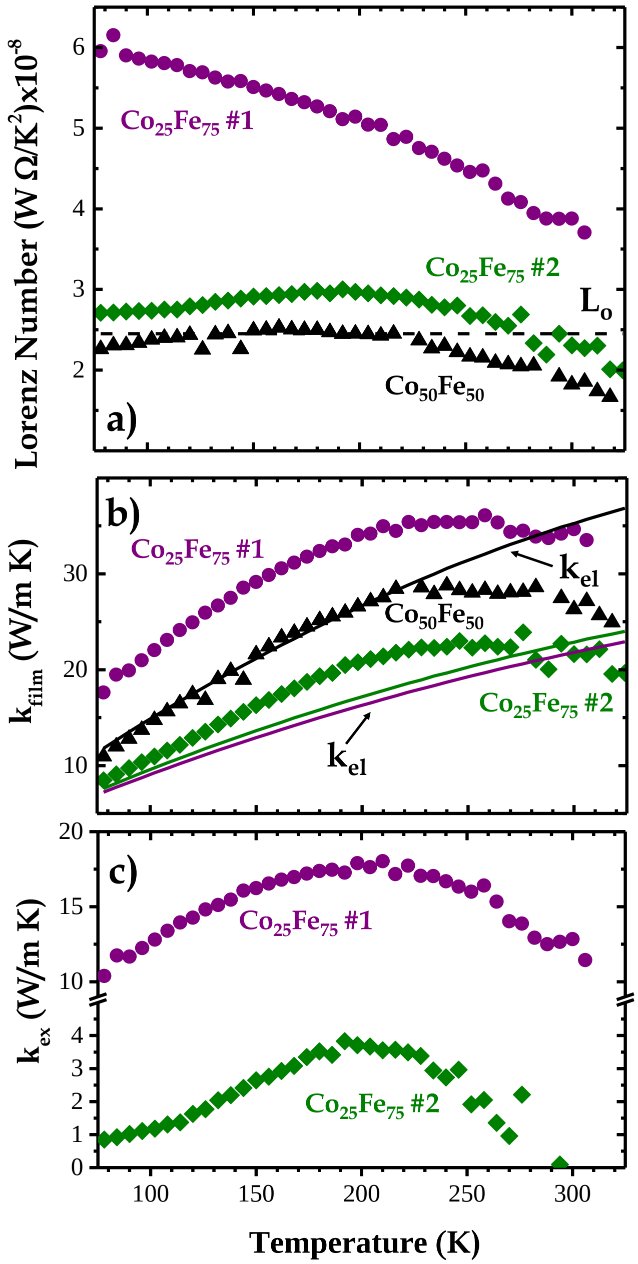

FIG. 2. **a)** $L = K_{\mathrm{S}}R/T$ vs. T for three $\mathrm{Co}_x\mathrm{Fe}_{1-x}$ films compared to L_o. The two low α films have dramatically increased L, indicating non-electronic contributions to k_{film}. **b)** $k_{\mathbf{film}}$ vs T for these samples, with estimated k_{el} also shown. **c)** The non-electronic contribution $k_{\mathrm{ex}} = k_{\mathrm{film}} - k_{\mathrm{el}}$ vs. T (left axis) for both $x = 25$ films show peaks near 200 K.

agrees with the WF exceptionally well by comparison. The lower k is expected based on disorder scattering from the random alloy in both cases. The two nominally similar $Co_{25}Fe_{75}$ films, which were grown in the same sputtering run on platforms held only several cm apart, have quite different k, though both significantly exceed k_{el}. We suspect that near the dip in DOS and α, k is strongly dependent on small fluctuations in alloy composition, which we confirmed via XRD (see Supplementary Materials). Further study will be needed to confirm the impact on k. In Fig. 2c) we estimate the excess, non-electronic contributions $k_{\mathrm{ex}} = k - k_{\mathrm{el}}$ for the $Co_{25}Fe_{75}$ films. As seen by another group [51], k_{ex} peaks near 200 K for both films, though sample #1 shows much larger k_{ex}. As described further in Supplemental Materials [58], we can use calculations of the expected contribution from the THz exchange-dominated magnons to estimate that the average mean free path of magnons, assuming all $k_{\mathbf{ex}}$ is due to exchange magnons, ranges from several to tens of nanometers.

Fig. 3a) shows R vs. H for $Co_{25}Fe_{75}$ #2 for both $H_{\perp}$ and $H_{\parallel}$ [59]. The resulting pattern is similar to the AMR effects well known for transition metal FM [60], though with some unusual hysteresis features that could also be related to magnons [61–63]. We plot the AMR ratio, $\Delta\rho/\rho_{\mathrm{av}} = (\rho_{\parallel} - \rho_{\perp})/((1/3)\rho_{\parallel} + (2/3)\rho_{\perp}$ vs. T in Fig. 3b). The AMR effect is less than 1%, smaller than typical transition metal FMs, and notably smaller in the low-damping alloy film. This is in line with the expectations of lower α, since AMR is driven by spin-orbit scattering that would also contribute to damping mechanisms. In Fig. 3c) we plot the field and field-direction dependence of k_{film} vs. T for sample $Co_{25}Fe_{75}$ #2, again comparing to the expected k_{el}. In saturating H in both directions, k_{film} is suppressed from $H = 0$ values. As also seen in the K_{tot} (Fig. 1c)), k_{film} also clearly depends on field direction. Fig. 3d) shows the contrasting data taken under identical experimental conditions for the reference $Co_{50}Fe_{50}$ sample, where data in $H = 0$, $H_{\parallel}$ and $H_{\perp}$ are all within error bars. In Fig. 3e) we plot the analogous ratio for field-direction dependent k; $\Delta k/k_{\mathrm{av}} = (k_{\parallel} - k_{\perp})/(\frac{1}{3}k_{\parallel} + \frac{2}{3}k_{\perp})$ vs. T for both films. The WF law predicts a field-dependent k_{el} in cases where AMR exists from the field-dependent k_{el}, which should be on the order of the AMR ratio, that has been measured in rare cases [64]. Fig. 3e) confirms that the field-direction dependence of the low-damping FM $Co_{25}Fe_{75}$ is dramatically larger, well more than 10× the AMR ratio across the measured T range, and exceeding 25% at the lowest temperatures.

We clarify that all data labeled with $H = 0$ was taken before any significant field was applied to the samples. To the best of our ability to determine (further details in Supple-

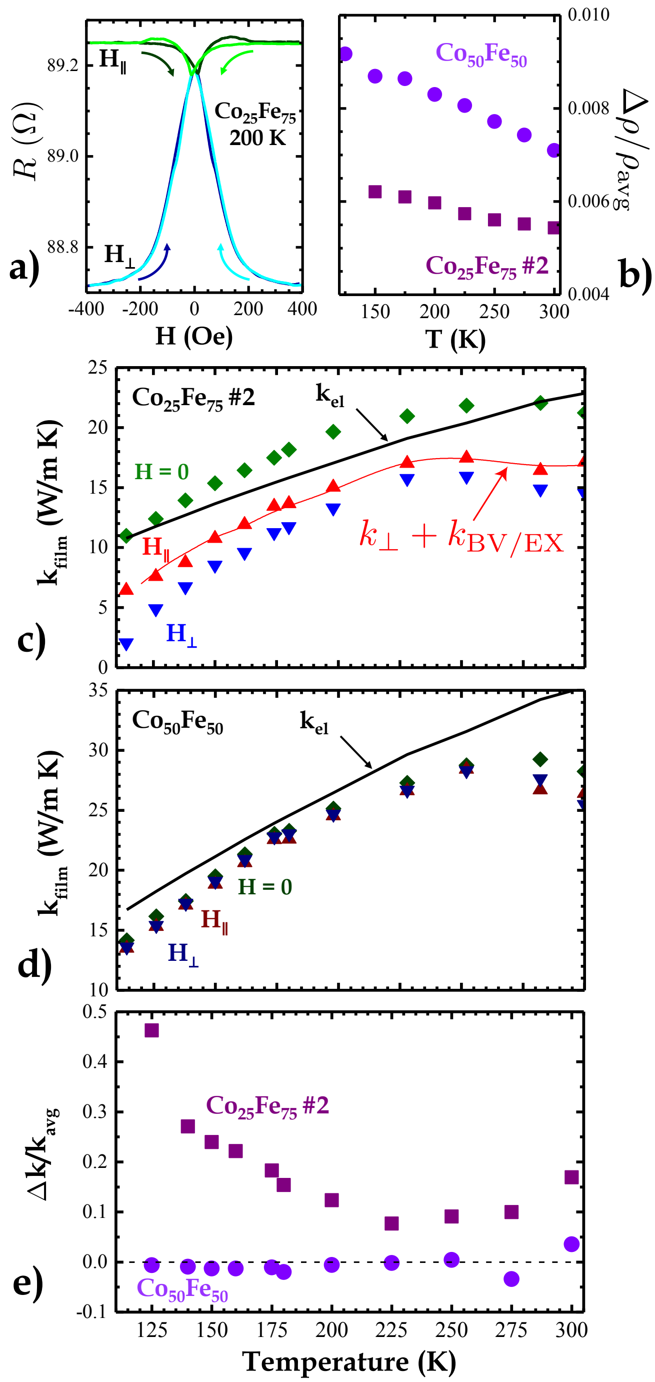

FIG. 3. **a)** R vs. H for $H_\perp$ and $H_\parallel$ for $Co_{25}Fe_{75}$ #2 at 200 K. **b)** AMR ratio vs T for $Co_{25}Fe_{75}$ #2 and $Co_{50}Fe_{50}$. **c)** $k_{\rm film}$ vs. T for $Co_{25}Fe_{75}$ #2 in $H = 0$, $H_\perp$ and $H_\parallel$ compared to $k_{\rm el}$ **d)** $k_{\rm film}$ vs. T for $Co_{50}Fe_{50}$ shows no change with field. **e)** The resulting anisotropic thermal conductivity ratio for $Co_{25}Fe_{75}$ #2 is $> 10\times$ larger than the AMR at all T, and exceeds 25% at low T.

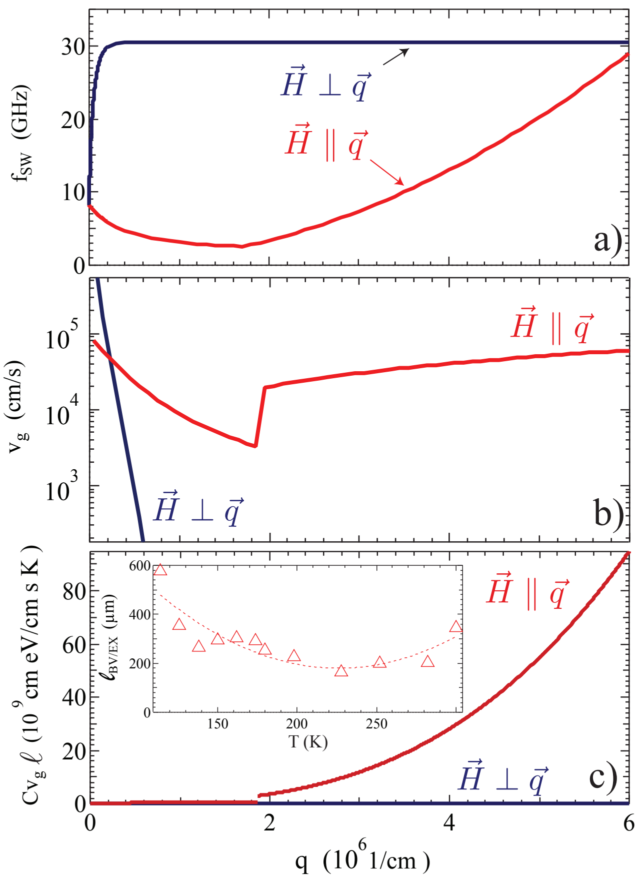

FIG. 4. **a)** Modeled spin wave dispersion curves, $f_{\rm sw}$ vs. q for low-q waves generated when $\vec{H} \perp \vec{q}$ (blue line), dominated by magnetostatic surface waves, and for waves generated when $\vec{H} \parallel \vec{q}$ (red lines), which arise from a combination of backward volume and exchange spin waves. **b)** Magnon group velocity, $v_{\rm g}$ determined from the dispersion relations. Note the discontinuity in the $\vec{H} \parallel \vec{q}$ case arises from our choice of the simplest possible model, and likely results in underestimation of $v_{\rm g}$ in this range of q, which could lead to an overestimate of ℓ. **c)** Integrating the curve shown here produced by the product $Cv_{\rm g}\ell$ vs. $\vec{q}$ gives $3k$, which shows that a significant contribution from these low q magnons comes only when $\vec{H} \parallel \vec{q}$. This curve used an assumed constant $\ell = 100$ μm. *Inset:* Estimated BVSW mean free path for the data of Fig. 3c.

mental Materials), after saturating field was applied to $Co_{25}Fe_{75}$ #2, $k_{\rm film}$ never returned to the initial values. However, this sample repeatably showed field direction dependence in the saturated state, as shown in Supplemental Materials [58]. This field-direction dependence suggests that the magnons causing the field direction-dependenent $k_{\rm film}$ involve spin waves with wavevector below $\vec{q} \sim 6 \times 10^6$ cm^{-1}, where the dispersion relations depend on the in-plane field direction [19, 65–68]. Above this $\vec{q}$ for our films, H direction independent exchange modes dominate. We show a simplified model of such field-direction dependent dispersion relations in Fig. 4a), calculated for our film using measured saturation magnetization and using reference values for the exchange constant [69, 70]. As detailed further in Supplemental Materials [58], this model captures the essential physics but does not use the fully correct theory of magnons at these wavelengths. As shown in Fig. 4a), for all non-zero $q < 10^6$ cm^{-1}, the spin wave frequency f_{SW} is higher when $\vec{H} \parallel q$ than when $\vec{H} \perp q$. q is the magnon wavevector which sets the propagation direction, which in our experiments is the direction of energy transport and therefore parallel to ∇T We determine contributions to k from this dispersion via $k = (1/3)Cv_{\mathrm{g}}\ell$, where C is the mode heat capacity, $v_g = d\omega/dq$ is the group velocity, and ℓ is the magnon mean free path. Note that this kinetic expression for k should be thought of as an integral over either wavevector or frequency, with all possible propagating excitations contributing, as seen in recent analogous work on phonon transport [71–75]. Fig. 4b) plots v_{g} vs. k, clarifying that in this picture, v_{g} is larger when $\vec{H} \parallel \vec{q}$ for all but the very lowest q magnons. Since C is the same for both modes (shown in Supplemental Materials [58]), this much larger v_{g} drives k higher for this field orientation. Fig. 4c plots the q-dependent product $Cv_{\mathrm{g}}\ell$, the integration of these curves gives the estimated field-direction dependent magnon k. Again, the much larger contribution when $\vec{H} \parallel \vec{q}$ is obvious, and integration of these curves indicates that magnons at these q essentially only contribute to k_{film} when $\vec{H} \parallel \nabla T$.

We can use this simple approach to estimate ℓ for our $Co_{25}Fe_{75}$ film. We calculated the solid red line in Fig. 3c) by adding the calculated $k_{\mathrm{BV/EX}}$, named for the combination of Backward-Volume (BV) spin waves and low-$\vec{q}$ exchange modes excited when $H \parallel \nabla T$, to the measured k_{film} with $\vec{H} \perp \nabla T$. In this calculation the average magnon mean free path ℓ is a free parameter, which we have assumed depends on T but is independent of frequency. We show the resulting estimated low $\vec{q}$ magnon $\ell_{\mathrm{BV/EX}}$ inset in Fig. 4c). The values are long compared to the average ℓ for the entire population of exchange spin waves, which is reasonable for these modes with wavelength that reaches hundreds of nm and thus are less sensitive to surface and defect scattering. This rough estimate of ℓ is approximately an order of magnitude larger than measured spin wave propagation lengths for 20 GHz spin waves in a much thinner $Co_{25}Fe_{75}$ film, grown by the same techniques and with low damping [49]. The detailed dependence of ℓ on f_{sw} and q is currently unknown to the best of our knowledge, but it is not unreasonable that some regimes of these low q magnons that should result in field-direction dependent k_{film} have even longer ℓ.

Finally, we note that though we have demonstrated what we feel is a plausible physical origin for the field direction dependence and large non-electronic thermal conductivity observed for $Co_{25}Fe_{75}$ and *not* for $Co_{50}Fe_{50}$, other interpretations of the physics of this behavior may be possible. Though an origin related to, for example, field-direction dependent phonon transport in this polycrystalline film, perhaps driven by magnetoelastic effects, would also be highly novel.

In summary, we have used micromachined thermal isolation platforms to measure k, R, and L for three Co_xFe_{1-x} thin films as a function of T, applied field, and field direction. Two films with compositions near a minimum in α show very large values of L compared to a film with higher α, and to typical metal films. A strongly field-direction dependent k in the low α composition suggests that the excess k is related to spin dynamics. Our ongoing work includes exploration of thermopower on the same samples and further probe of thermal and spin effects in this unique system.

I. ACKNOWLEDGMENTS

We thank X. Fan, M. J. Roos, S. Bleser, and L. Hernandez for helpful discussions and/or assistance in the lab, J. Nogan and the IL staff at CINT for guidance and training in fabrication techniques, and gratefully acknowledge support from the NSF (DMR-1709646). This work was performed, in part, at the Center for Integrated Nanotechnologies, an Office of Science User Facility operated for the U.S. Department of Energy (DOE) Office of Science by Los Alamos National Laboratory (Contract DE-AC52-06NA25396) and Sandia National Laboratories (Contract DE-AC04-94AL85000).

[1] R. Franz and G. Wiedemann, Ueber die wärme-leitungsfähigkeit der metalle, Annalen der Physik und Chemie **165**, 497 (1853).

[2] L. Lorenz, Bestimmung der wärmegrade in absolutem maasse, Annalen der Physik und Chemie **223**, 429 (1872).

[3] G. S. Kumar, G. Prasad, and R. O. Pohl, Experimental determinations of the Lorenz number, Journal of Materials Science **28**, 4261 (1993).

[4] A. Jain and A. J. H. McGaughey, Thermal transport by phonons and electrons in aluminum, silver, and gold from first principles, Phys. Rev. B **93**, 081206 (2016).

[5] Y. Wang, Z. Lu, and X. Ruan, First principles calculation of lattice thermal conductivity of metals considering phonon-phonon and phonon-electron scattering, Journal of Applied Physics **119**, 225109 (2016).

[6] Z. Tong, S. Li, X. Ruan, and H. Bao, Comprehensive first-principles analysis of phonon thermal conductivity and electron-phonon coupling in different metals, Phys. Rev. B **100**, 144306 (2019).

[7] L. Lindsay, A. Katre, A. Cepellotti, and N. Mingo, Perspective on ab initio phonon thermal transport, Journal of Applied Physics **126**, 050902 (2019).

[8] N. T. Eigenfeld, J. C. Gertsch, G. D. Skidmore, S. M. George, and V. M. Bright, Electrical and thermal conduction in ultra-thin freestanding atomic layer deposited W nanobridges, Nanoscale **7**, 17923 (2015).

[9] A. D. Avery, S. J. Mason, D. Bassett, D. Wesenberg, and B. L. Zink, Thermal and electrical conductivity of approximately 100-nm permalloy, Ni, Co, Al, and Cu films and examination of the Wiedemann-Franz law, Phys. Rev. B **92**, 214410 (2015).

[10] M. N. Ou, T. J. Yang, S. R. Harutyunyan, Y. Y. Chen, C. D. Chen, and S. J. Lai, Electrical and thermal transport in single nickel nanowire, Applied Physics Letters **92**, 063101 (2008).

[11] Q. G. Zhang, B. Y. Cao, X. Zhang, M. Fujii, and K. Takahashi, Influence of grain boundary scattering on the electrical and thermal conductivities of polycrystalline gold nanofilms, Phys. Rev. B **74**, 134109 (2006).

[12] A. A. Serga, A. V. Chumak, and B. Hillebrands, YIG magnonics, Journal of Physics D: Applied Physics **43**, 264002 (2010).

[13] A. V. Chumak, A. A. Serga, M. B. Jungfleisch, R. Neb, D. A. Bozhko, V. S. Tiberkevich, and B. Hillebrands, Direct detection of magnon spin transport by the inverse spin Hall effect, Applied Physics Letters **100**, 082405 (2012).

[14] L. J. Cornelissen, J. Liu, R. A. Duine, J. B. Youssef, and B. J. van Wees, Long-distance transport of magnon spin information in a magnetic insulator at room temperature, Nat Phys **11**, 1022 (2015).

[15] S. T. B. Goennenwein, R. Schlitz, M. Pernpeintner, K. Ganzhorn, M. Althammer, R. Gross, and H. Huebl, Non-local magnetoresistance in YIG/Pt nanostructures, Appl. Phys. Lett. **107**, 172405 (2015).

[16] J. Cramer, E.-J. Guo, S. Geprägs, A. Kehlberger, Y. P. Ivanov, K. Ganzhorn, F. D. Coletta, M. Althammer, H. Huebl, R. Gross, J. Kosel, M. Kläui, and S. T. B. Goennenwein, Magnon mode selective spin transport in compensated ferrimagnets, Nano Letters **17**, 3334 (2017).

[17] B. L. Giles, Z. Yang, J. S. Jamison, and R. C. Myers, Long-range pure magnon spin diffusion observed in a nonlocal spin-Seebeck geometry, Phys. Rev. B **92**, 224415 (2015).

[18] N. Thiery, A. Draveny, V. V. Naletov, L. Vila, J. P. Attané, C. Beigné, G. de Loubens, M. Viret, N. Beaulieu, J. Ben Youssef, V. E. Demidov, S. O. Demokritov, A. N. Slavin, V. S. Tiberkevich, A. Anane, P. Bortolotti, V. Cros, and O. Klein, Nonlinear spin conductance of yttrium iron garnet thin films driven by large spin-orbit torque, Phys. Rev. B **97**, 060409 (2018).

[19] A. V. Chumak, V. I. Vasyuchka, A. A. Serga, and B. Hillebrands, Magnon spintronics, Nat Phys **11**, 453 (2015).

[20] V. V. Kruglyak, S. O. Demokritov, and D. Grundler, Magnonics, Journal of Physics D: Applied Physics **43**, 264001 (2010).

[21] M. Madami, S. Bonetti, G. Consolo, S. Tacchi, G. Carlotti, G. Gubbiotti, F. B. Mancoff, M. A. Yar, and J. Åkerman, Direct observation of a propagating spin wave induced by spin-transfer torque, Nature Nanotechnology **6**, 635 (2011).

[22] B. Lenk, H. Ulrichs, F. Garbs, and M. Münzenberg, The building blocks of magnonics, Physics Reports **507**, 107 (2011).

[23] N. Prasai, B. A. Trump, G. G. Marcus, A. Akopyan, S. X. Huang, T. M. McQueen, and J. L. Cohn, Ballistic magnon heat conduction and possible Poiseuille flow in the helimagnetic insulator Cu_2OSeO_3, Phys. Rev. B **95**, 224407 (2017).

[24] S. R. Boona and J. P. Heremans, Magnon thermal mean free path in yttrium iron garnet, Phys. Rev. B **90**, 064421 (2014).

[25] B. Y. Pan, T. Y. Guan, X. C. Hong, S. Y. Zhou, X. Qiu, H. Zhang, and S. Y. Li, Specific heat and thermal conductivity of ferromagnetic magnons in yttrium iron garnet, EPL (Europhysics Letters) **103**, 37005 (2013).

[26] C. Hess, B. Büchner, U. Ammerahl, L. Colonescu, F. Heidrich-Meisner, W. Brenig, and A. Revcolevschi, Magnon heat transport in doped La_2CuO_4, Phys. Rev. Lett. **90**, 197002 (2003).

[27] R. Jin, Y. Onose, Y. Tokura, D. Mandrus, P. Dai, and B. C. Sales, In-plane thermal conductivity of Nd_2CuO_4: Evidence for magnon heat transport, Physical Review Letters **91**, 146601 (2003).

[28] C. M. Bhandari and G. S. Verma, Scattering of magnons and phonons in the thermal conductivity of yttrium iron garnet, Physical Review **152**, 731 (1966).

[29] R. L. Douglass, Heat transport by spin waves in yttrium iron garnet, Phys. Rev. **129**, 1132 (1963).

[30] Y. Hsu and L. Berger, Magnon heat conduction and magnon lifetimes in the metallic ferromagnet $Fe_{68}Co_{32}$ at low temperatures, Phys. Rev. B **14**, 4059 (1976).

[31] Y. Hsu and L. Berger, Transport of heat by spin waves in $Fe_{95}Si_5$, Phys. Rev. B **18**, 4856 (1978).

[32] W. B. Yelon and L. Berger, Magnon heat conduction and magnon scattering processes in Fe-Ni alloys, Phys. Rev. B **6**, 1974 (1972).

[33] H. W. Gronert, D. M. Herlach, and E. F. Wassermann, Evidence of magnon thermal transport in a ferromagnetic glassy metal, Europhysics Letters (EPL) **6**, 641 (1988).

[34] X. Wu, Z. Liu, and T. Luo, Magnon and phonon dispersion, lifetime, and thermal conductivity of iron from spin-lattice dynamics simulations, Journal of Applied Physics **123**, 085109 (2018).

[35] Y. Zhou, J. Tranchida, Y. Ge, J. Murthy, and T. S. Fisher, Atomistic simulation of phonon and magnon thermal transport across the ferromagnetic-paramagnetic transition, Phys. Rev. B **101**, 224303 (2020).

[36] Y. Tserkovnyak, S. A. Bender, R. A. Duine, and B. Flebus, Bose-einstein condensation of magnons pumped by the bulk spin Seebeck effect, Phys. Rev. B **93**, 100402 (2016).

[37] B. Flebus, R. A. Duine, and Y. Tserkovnyak, Landau-Lifshitz theory of the magnon-drag thermopower, EPL (Europhysics Letters) **115**, 57004 (2016).

[38] H. Chen, A. D. Kent, A. H. MacDonald, and I. Sodemann, Nonlocal transport mediated by spin supercurrents, Phys. Rev. B **90**, 220401 (2014).

[39] M. E. Lucassen, C. H. Wong, R. A. Duine, and Y. Tserkovnyak, Spin-transfer mechanism for magnon-drag thermopower, Applied Physics Letters **99**, 262506 (2011).

[40] S. J. Watzman, R. A. Duine, Y. Tserkovnyak, S. R. Boona, H. Jin, A. Prakash, Y. Zheng, and J. P. Heremans, Magnon-drag thermopower and Nernst coefficient in Fe, Co, and Ni, Phys. Rev. B **94**, 144407 (2016).

[41] M. V. Costache, G. Bridoux, I. Neumann, and S. O. Valenzuela, Magnon-drag thermopile, Nature Materials **11**, 199 (2012).

[42] M. A. W. Schoen, D. Thonig, M. L. Schneider, T. J. Silva, H. T. Nembach, O. Eriksson, O. Karis, and J. M. Shaw, Ultra-low magnetic damping of a metallic ferromagnet, Nature Physics **12**, 839 (2016).

[43] The assumption that the Gilbert damping parameter, which is determined from resonant excitation of the non-propagating uniform precession mode, is representative of the broader spectrum of spin waves is fairly common. For further comment, see Supplemental Materials.

[44] C. Liu, C. K. A. Mewes, M. Chshiev, T. Mewes, and W. H. Butler, Origin of low Gilbert damping in half metals, Applied Physics Letters **95**, 022509 (2009).

[45] S. Andrieu, A. Neggache, T. Hauet, T. Devolder, A. Hallal, M. Chshiev, A. M. Bataille, P. Le Fèvre, and F. m. c. Bertran, Direct evidence for minority spin gap in the Co_2MnSi Heusler compound, Phys. Rev. B **93**, 094417 (2016).

[46] A. J. Lee, J. T. Brangham, Y. Cheng, S. P. White, W. T. Ruane, B. D. Esser, D. W. McComb, P. C. Hammel, and F. Yang, Metallic ferromagnetic films with magnetic damping under 1.4 $\times 10^{-3}$, Nature Communications **8**, 234 (2017).

[47] J. M. Shaw, E. K. Delczeg-Czirjak, E. R. J. Edwards, Y. Kvashnin, D. Thonig, M. A. W. Schoen, M. Pufall, M. L. Schneider, T. J. Silva, O. Karis, K. P. Rice, O. Eriksson, and H. T. Nembach, Magnetic damping in sputter-deposited Co_2MnGe Heusler compounds with A2,B2 , and L21 orders: Experiment and theory, Physical Review B **97**, 094420 (2018).

[48] D. A. Smith, A. Rai, Y. Lim, T. Q. Hartnett, A. Sapkota, A. Srivastava, C. Mewes, Z. Jiang, M. Clavel, M. K. Hudait, D. D. Viehland, J. J. Heremans, P. V. Balachandran, T. Mewes, and S. Emori, Magnetic damping in epitaxial iron alloyed with vanadium and aluminum, Phys. Rev. Applied **14**, 034042 (2020).

[49] L. Flacke, L. Liensberger, M. Althammer, H. Huebl, S. Geprägs, K. Schultheiss, A. Buzdakov, T. Hula, H. Schultheiss, E. R. J. Edwards, H. T. Nembach, J. M. Shaw, R. Gross, and M. Weiler, High spin-wave propagation length consistent with low damping in a metallic ferromagnet, Applied Physics Letters **115**, 122402 (2019).

[50] Y. Zheng, E. J. Weiss, N. Antolin, W. Windl, and J. P. Heremans, Magnon drag effect in Fe-Co alloys, Journal of Applied Physics **126**, 125107 (2019).

[51] S. Srichandan, S. Wimmer, S. Pöllath, M. Kronseder, H. Ebert, C. H. Back, and C. Strunk, Magnon scattering in the transport coefficients of CoFe thin films, Phys. Rev. B **98**, 020406 (2018).

[52] G. Wehmeyer, T. Yabuki, C. Monachon, J. Wu, and C. Dames, Thermal diodes, regulators, and switches: Physical mechanisms and potential applications, Applied Physics Reviews **4**, 041304 (2017).

[53] S. Husain, S. Akansel, A. Kumar, P. Svedlindh, and S. Chaudhary, Growth of Co_2FeAl Heusler alloy thin films on Si(100) having very small Gilbert damping by ion beam sputtering, Scientific Reports **6**, 28692 (2016).

[54] E. R. Edwards, H. T. Nembach, and J. M. Shaw, $Co_{25}Fe_{75}$ thin films with ultralow total damping of ferromagnetic resonance, Phys. Rev. Applied **11**, 054036 (2019).

[55] S. J. Mason, D. J. Wesenberg, A. Hojem, M. Manno, C. Leighton, and B. L. Zink, Violation of the Wiedemann-Franz law through reduction of thermal conductivity in gold thin films, Phys. Rev. Materials **4**, 065003 (2020).

[56] R. Sultan, A. D. Avery, J. M. Underwood, S. J. Mason, D. Bassett, and B. L. Zink, Heat transport by long mean free path vibrations in amorphous silicon nitride near room temperature, Phys. Rev. B **87**, 214305 (2013).

[57] R. Sultan, A. D. Avery, G. Stiehl, and B. L. Zink, Thermal conductivity of micromachined low-stress silicon-nitride beams from $77 - 325$ K, Journal of Applied Physics **105**, 043501 (2009).

[58] See Supplemental Material at [URL will be inserted by publisher] for additional details on Si-N membrane thermal conductivity measurements, repeatability of field-direction dependence, resistivity, AMR, XRD of Co-Fe films, and additional details on the model for how low-q magnons contribute to thermal conductivity.

[59] The micromachined platform supporting $Co_{25}Fe_{75}$ #1 broke before we could perform field-dependent measurements on this sample.

[60] T. R. McGuire and R. I. Potter, Anisotropic magnetoresistance in ferromagnetic 3d alloys, IEEE Transactions on Magnetics **MAG-11**, 1018 (1975).

[61] A. P. Mihai, J. P. Attané, A. Marty, P. Warin, and Y. Samson, Electron-magnon diffusion and magnetization reversal detection in FePt thin films, Phys. Rev. B **77**, 060401 (2008).

[62] V. D. Nguyen, C. Naylor, L. Vila, A. Marty, P. Laczkowski, C. Beigné, L. Notin, Z. Ishaque, and J. P. Attané, Magnon magnetoresistance of NiFe nanowires: Size dependence and domain wall detection, Applied Physics Letters **99**, 262504 (2011).

[63] V. D. Nguyen, L. Vila, P. Laczkowski, A. Marty, T. Faivre, and J. P. Attané, Detection of domain-wall position and magnetization reversal in nanostructures using the magnon contribution to the resistivity, Phys. Rev. Lett. **107**, 136605 (2011).

[64] J. Kimling, J. Gooth, and K. Nielsch, Anisotropic magnetothermal resistance in Ni nanowires, Phys. Rev. B **87**, 094409 (2013).

[65] A. D. Karenowska, A. V. Chumak, A. A. Serga, and B. Hillebrands, Magnon spintronics, in *Handbook of Spintronics* (Springer Netherlands, 2016) pp. 1505–1549.

[66] S. Neusser and D. Grundler, Magnonics: Spin waves on the nanoscale, Advanced Materials **21**, 2927 (2009).

[67] U. K. Bhaskar, G. Talmelli, F. Ciubotaru, C. Adelmann, and T. Devolder, Backward volume vs Damon–Eshbach: A traveling spin wave spectroscopy comparison, Journal of Applied Physics **127**, 033902 (2020).

[68] R. W. Damon and J. R. Eshbach, Magnetostatic modes of a ferromagnetic slab, Journal of Applied Physics **31**, S104 (1960).

[69] C. Eyrich, W. Huttema, M. Arora, E. Montoya, F. Rashidi, C. Burrowes, B. Kardasz, E. Girt, B. Heinrich, O. N. Mryasov, M. From, and O. Karis, Exchange stiffness in thin film Co alloys, Journal of Applied Physics **111**, 07C919 (2012).

[70] C. Eyrich, *Exchange Stiffness in Thin-Film Cobalt Alloys*, Ph.D. thesis, Simon Frasier University (2012).

[71] Y. K. Koh and D. G. Cahill, Frequency dependence of the thermal conductivity of semiconductor alloys, Phys. Rev. B **76**, 075207 (2007).

[72] A. J. Minnich, J. A. Johnson, A. J. Schmidt, K. Esfarjani, M. S. Dresselhaus, K. A. Nelson, and G. Chen, Thermal conductivity spectroscopy technique to measure phonon mean free paths, Phys. Rev. Lett. **107**, 095901 (2011).

[73] A. J. Minnich, Determining phonon mean free paths from observations of quasiballistic thermal transport, Phys. Rev. Lett. **109**, 205901 (2012).

[74] K. T. Regner, D. P. Sellan, Z. Su, C. H. Amon, A. J. H. McGaughey, and J. A. Malen, Broadband phonon mean free path contributions to thermal conductivity measured using frequency domain thermoreflectance, Nature Communications **4**, 1640 (2013).

[75] J. M. Larkin and A. J. H. McGaughey, Thermal conductivity accumulation in amorphous silica and amorphous silicon, Phys. Rev. B **89**, 144303 (2014).